Bulk Molybdenum Spindt Field Emission Arrays

Ningli Zhu[a], Kaisi Xu[a], Yusheng Zhai[b], Zhi Tao[b], Yunsong Di[c], Zhipeng Zhang[d], Jun Chen[d], Matthew T. Cole[e], William I. Milne[e], & Jing Chen[a]*

[a]*Institute of Microelectronics, Peking University, Beijing, China*
[b]*School of Electronic Science & Engineering, Southeast University, Nanjing, China*
[c]*School of Physics and Technology,Nanjing Normal University, Nanjing, China*
[d]*State Key Laboratory of Optoelectronic Materials and Technologies, Sun Yat-Sen University, Guangzhou, China*
[e]*Electrical Engineering, Department of Engineering, University of Cambridge, United Kingdom*

ABSTRACT

This paper reports on a simple approach for fabricating modest aspect ratio field emission arrays (FEAs) directly from bulk molybdenum substrates via the use of fluorine inductive-coupled-plasma (ICP) etching. Compared to traditional Spindt array fabrication, through our outlined fabrication process all thin film interfaces have been eliminated reducing tip delamination during operation. The as-fabricated devices exhibited low turn-on electric fields (I = 100nA) of 1.21 V/µm. Arrays of more than 10^6 tips, with controlled inter-tip-pitches of 10 µm, have produced maximum currents of up to 140 µA (5.48 V/µm). Spatially uniform emission, that can be white light optically modulated, has been observed making our Mo-FEAs promising for use in long-term, high beam current continuous emission applications.

I. INTRODUCTION

Electron emission is central to a wide range of systems, including microwave amplifiers, X-ray sources, displays, and travelling wave tubes[1, 2]. To date, field emission arrays (FEA) within many of these systems have been formed by either conventional Spindts, micro-sized cones fabricated by conventional top-down processes, or, more recently, through the bottom-up direct synthesis of one-dimensional nanostructures[3]. Nanoengineered devices are increasingly coming to the fore[4, 5], nevertheless Spindt emitters continue to dominate the commercial landscape at present. Due to geometric field enhancement, micro-Spindt emitters create high electric fields at relatively low voltages. However, in conventional devices the deposited Mo often delaminates during operation due to the low substrate-emitter adhesion and aggressive operating conditions. Moreover, traditional fabrication processes have been shown to be complex and costly[6]. Major manufacturing challenges remain. Chief amongst these lies in achieving high fabrication yields, alongside spatially and temporally uniform emission. The low work function and high melting temperature of Mo have made it a common material of choice for many Spindt emitters and a high yield process for the fabrication of large-area FEAs from bulk metals is required for rapid industrial adoption. With careful design and further optimisation of the fabrication process presented we believe that the outlined methodology herein will allow us to realise increasingly uniform arrays of micro-tips from bulk metals, and a platform that will allow for increasingly high beam currents, especially when coupled with emerging nanomaterial-based adlayers and over-coating schemes which have been shown to further enhance the emission current at a given bais[7].

Our bulk Mo–FEA fabrication process is reported in detail elsewhere[8]. In brief, and as shown in **Figure 1**, a double-side-polished 400 µm thick, 4-inch high purity Mo wafer was first coated with an evaporated 500 nm thick Al film to form an etching hard mask (**Figure 1b**). Tip arrays were subsequently patterned by photolithography (**Figure 1c-d**), with the Al patterned by dry-etching in CH_3F plasma (**Figure 1e**). The Mo-FEA tips were etched using an anisotropic SF_6/Ar dry etch in a commercial ICP etcher (**Figure 1**). Ultrasonication (15 W) for 60s was

employed to remove residual Al following the ICP etch (**Figure 1g**). Various geometries of etching hard mask; including circular, triangular, square, hexagonal, and octagonal; each of different size, were considered, resulting in nominal tip heights ranging between 4-8 µm. As shown in **Figure 1h**, Mo–FEAs with a pitch of 5 µm were realized with high spatial uniformity and aspect ratios consistently > 10, with a typical mean tip radius of 25.5 nm. The aspect ratios attainable limit the breadth of application of the outlined procedure, especially when compared to emerging 1D nanostructures. Though further enhancement to the aspect ratio is indeed possible through additional process optimisation, values comparable to those attained readily for carbon nanotubes and nanowires, for example, remain particularly challenging to achieve. Nevertheless, the outline generalised fabrication procedure offers a low cost means with rapid integration into incumbent systems, with ICP etching of W, Ti and other technologically relevant electron emission metals possible.

Field emission is described as the quantum mechanical tunnelling of conduction electrons through the surface potential barrier under the influence of a high electric field[9, 10]. For bulk metals, the current density, J, can be calculated using conventional Fowler-Nordheim (FN) theory, as;

$$J = \frac{AF_t^2}{\phi t(f)^2} \exp[-B\frac{\phi^{3/2}}{F_t}v(f)] \tag{1}$$

Here F_t is the electric field at the tip apex, ϕ the emitter surface work function, and A (= 1.54 µA.eV.V^2) and B (= 6.83 eV$^{-3/2}$.V.nm^{-1}) are constants. t(f) and v(f) are the purely mathematical, slowly varying dimensionless Nordheim elliptical functions. f is the slope correction factor. For simplicity v(f) is most often set to unity with minimal loss in accuracy and;

$$t(f)=(3.79\text{x}10^{-5})F^{\frac{1}{2}}/\phi \tag{2}$$

Equation (1) may be expressed in terms of $F_t = \beta(V/\text{d})$, where V is the applied potential and d is the cathode-anode gap. β is termed the field enhancement factor; the factor through which the local electric field is geometrically enhanced, and may be linearly approximated as $\beta = h/r$, where h is the height of the tip and r is the radius of curvature at the tip apex. Though an approximate model, the emission current is nonetheless intimately related to the work function of the emitting surface, the radius of the emitting apex and the emission area; though the exact weighting on each of these parameters remains largely unclear in the sub-micro and nano regimes even in the case of metallic emitters. Nevertheless, for a fixed emitter geometry, at a fixed electric field, lowering of the emitters work function will certainly stimulate an increase in emission current. For bulk metals the field emission current is well estimated by established FN theory[11, 12]. In such systems, the emitter geometry greatly influences the magnitude of the local electric field and the electron energy distribution.
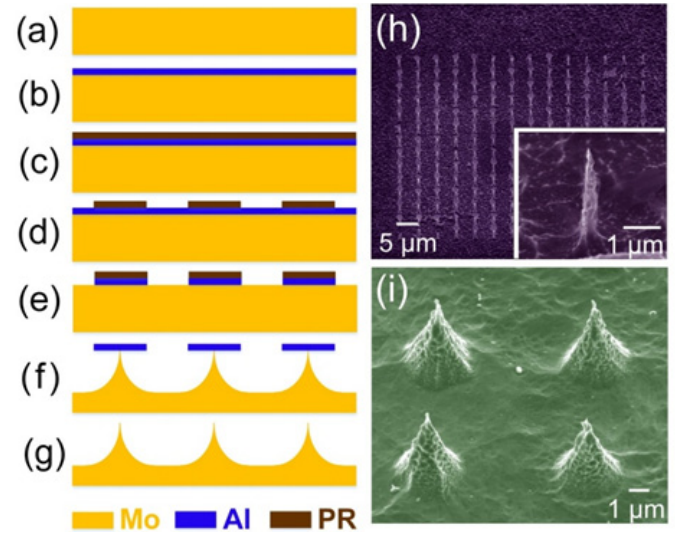

Figure 1 (a-g) Cross-sectional scheme depicting the fabrication of the bulk Mo-FEAs. Scanning electron micrographs of **(h)** an Al-masked (2.5 µm) Mo-FEA (scale bar: 5 µm), *inset* depicts a typical single tip (scale bar: 1 µm), and a **(i)** Mo-FEA with the Al mask removed (mask diameter = 4.5 µm) (scale bar: 1 µm).

The two central geometric properties influencing the emission performance are the apex radius and the tip aspect ratio, as illustrated in **Figure 2a**.
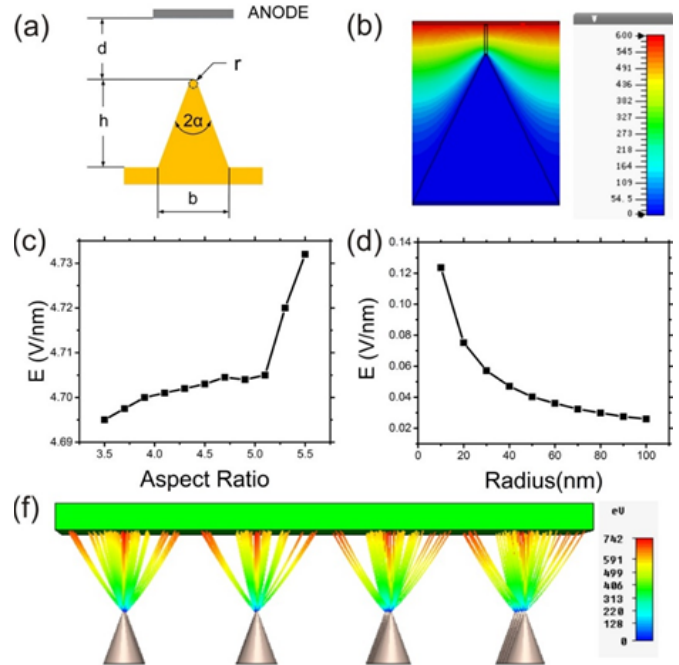

Figure 2 (a) Schematic depicting the critical tip geometries affecting the observed field electron emission. **(b)** Simulated electric field distribution, and electric field as a function of; **(c)** emitter aspect ratio, and **(d)** tip radius. **(f)** Corresponding electron trajectories at an anode bias of 600 V.

We have modelled the three-dimensional electrostatic field for our nominal emitter geometries. As show in **Figure 2b, c**, a tip radius of 40 nm was used whilst in the simulation in **Figure 2d** a tip radius

range of 10-100 nm was considered. The larger tip radius was chosen to examine the effects of tip height on field strength, as it is representative of a more reasonable manufacturing goal. A typical tips electric field contour distribution, F_{tip}, is shown in **Figure 2b**. **Figure 2c, d** shows the relationships between the Mo–FEAs' geometry and F_{tip}. As elsewhere, we find that the electric field increases with aspect ratio and that a sharp tip (low radius of curvature) beneficially increases the local electric field. **Figure 2f** shows our simulated electron emission trajectories for the Mo-FEAs for a standard operating fixed anode voltage of 600 V. In the far field, where the inter-electrode gap is significantly larger than the tip-to-tip pitch, we note large Coloumbic interactions resulting in a high beam divergence.
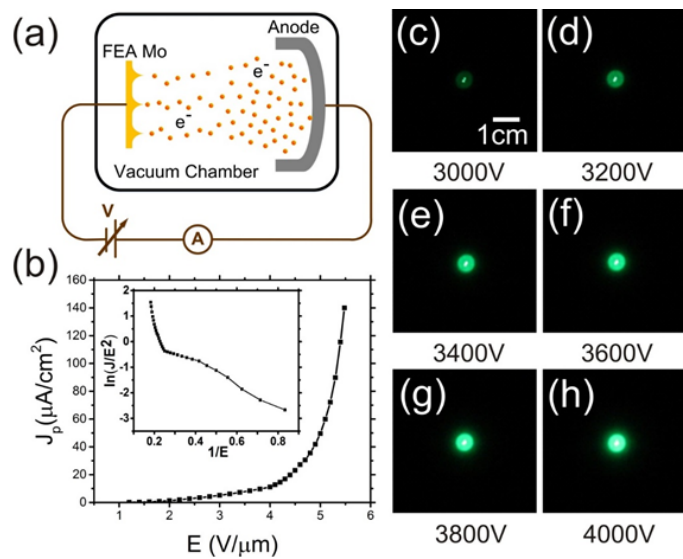
mm^2 was used throughout. To ensure thorough out-gassing, samples were pre-heated to 300°C for 5h under vacuum. The field emission current density reached a maximum of 140 $\mu A/cm^2$ at 5.48 V/μm. The measured emission conforms well to FN behaviour (R^2 = 0.960). Though the measured current densities fall short of travelling wave tube and Xray applications, our low-cost devices remain nonetheless competitive and useful for display applications, advanced space propulsion systems, and gas sensors, that latter of which is particularly attractive given the relative stability of oxidised Mo. The corresponding FN plot, from an array of 1000 x 1000 emitters, is shown in the inset of **Figure 3b**. **Figure 3(c-h)** show integrated intensity maps of the Mo-FEAs at applied bias of 3-4 kV. At low electric fields, there appear a few dominant emission site, suggesting some possible non-uniformity in tip geometry. We find that as the applied bias tends to increase the integrated intensity maps become increasingly uniform, likely due to saturation of the phosphor and mounted CCD. Further studies are underway to better understand the underlying mechanisms for this observed spatial variation.

Figure 3 (a) Schematic of the field emission measurement system. **(b)** J-E curves of Mo-FEAs. *Inset:* Corresponding FN plot. **(c-h)** Integrated intensity maps as a function of anode voltage, as stated (scale bar: 1 cm).

Figure 3a shows a schematic of the field electron emission experimental setup. Here, the Mo-FEAs form the cathode, which was placed adjacent to a phosphor coated ITO/glass anode, all within a vacuum chamber evacuated to a base pressure of 10^{-8} mbar and attached to a source measure unit. The anode-cathode distance was 600 μm. All samples were measured in a simple diode configuration. An emission area of 100

As shown in **Figure 4a**, optical excitation tests were conducted *in situ* using four micro-anode probes and a white-optical-source, all equipped within a standard SEM chamber operated at a base pressure of 3×10^{-5} mbar. Samples were irradiated with a white light source with an inclusive wavelength of 300-700 nm[13]. **Figure 4b** shows the two tungsten probes utilized as the anode and ground probes, respectively. The light-dependent electron emission from the cathode was investigated using a tungsten probe anode carefully placed adjacent (5 μm above the sample) to four Mo micro-tips (**Figure 4c**). **Figure 4d** shows typical measured I-V data during optical excitation. The curves A to C represent the electron emission with no illumination (termed 'Dark'). The curves α to γ are those under white illumination (termed 'Light'). Though direct comparisons between our earlier parallel plate measurements cannot be made, we note that the maximum emission current under optical excitation is evidently larger than without illumination. The average maximum emission current from a single Mo micro-tip under white optical excitation was 11 μA, some 1.4 times
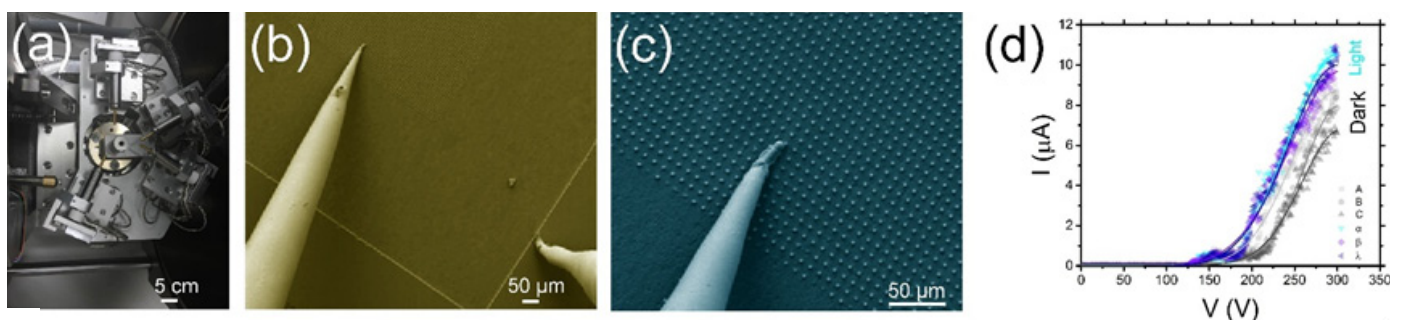

Figure 4 (a) Scanning electron microscope mounted *In-situ* micro-anode probes (scale bar: 5 cm). False coloured scanning electron micrographs of; **(b)** the tungsten anode and ground tips (scale bar: 50 μm), and **(c)** magnified view (scale bar: 50 μm). **(d)** I-V curves of Mo micro tips with and without optical excitation.

larger than that of the non-illuminated tips (7.8µA). We attribute this to further local field enhancement of the plasmonically active sub-micron tips, though we are continuing to study further the underlying mechanisms behind this observed optical enhancement.

II. CONCLUSION

Here we have presented our on-going work on the fabrication and operation of field emission micro-tip arrays based on bulk Mo. Electrostatic simulations showed a strong positive correlation between the local tip electric field and the tip aspect ratio, whilst highlighting an increase in tip field with reduced tip radius of curvature. Mo-FEA fabrication, using bulk micro-machining technology, has been demonstrated and the emission performance validated. The as-fabricated devices showed a low turn-on electric field of 1.21 V/µm, with FEAs consisting of more than 10^6 tips producing a maximum current of up to 140 µA, which showed further enhancement during white broadband optical excitation.

III. ACKNOWLEDGEMENTS

IV. REFERENCES

1. Koh, A. T. T.; Foong, Y. M.; Yusop, Z.; Tanemura, M.; Chua, D. H. C. *Advanced Materials Interfaces* **2014,** 1, (5).
2. Pekarek, J.; Vrba, R.; Prasek, J.; Jasek, O.; Majzlikova, P.; Pekarkova, J.; Zajickova, L. *IEEE Sensors Journal* **2015,** 15, (3), 1430-1436.
3. Cole, M. T.; Teo, K. B. K.; Groening, O.; Gangloff, L.; Legagneux, P.; Milne, W. I. *Scientific Reports* **2014,** 4, (4840).
4. Cole, M. T.; Hou, K.; Warner, J. H.; Barnard, J. S.; Ying, K.; Zhang, Y.; Li, C.; Teo, K. B. K.; Milne, W. I. *Diamond and Related Materials.* **2012,** 23, 66-71.
5. Cole, M. T.; Li, C.; Zhang, Y.; Shivareddy, S. G.; Barnard, J. S.; Lei, W.; Wang, B.; Pribat, D.; Amaratunga, G. A. J.; Milne, W. I. *ACS Nano* **2012,** 6, (4), 3236-3242.
6. Nagao, M.; Yoshizawa, S. In *Fabrication of spindt-type double-gated field-emitters using photoresist lift-off layer*, Vacuum Nanoelectronics Conference (IVNC), 2014 27th International, 2014.
7. Bell, M. S.; Teo, K. B. K.; Milne, W. I. *Journal of Physics D* **2007,** 40, (8), 2285-2292.
8. Chen, J.; Hu, J.; Zhang, Y.; Chen, S.; He, S.; Li, N. In *Inductively coupled plasma etching of bulk molybdenum*, Proceedings of the IEEE International Conference on Micro Electro Mechanical Systems, 2012; pp 267-270.
9. Fowler, R. H.; Nordheim, L. *Royal Society of London Proceedings* **1928,** 119, (781), 173-181.
10. Xu, N. S.; Huq, S. E. *Materials Science & Engineering R Reports* **2005,** 48, (s 2–5), 47-189.
11. Brodie, I.; Spindt, C. A. *Applications of Surface Science* **1979,** 2, (2), 149-163.
12. Spindt, C. A. *Surface Science* **1992,** 266, (1), 145-154.
13. Mustonen, A.; Beaud, P.; Kirk, E.; Feurer, T.; Tsujino, S. *Scientific Reports* **2012,** 2, (12), 915-915.